RSC Advances

PAPER

View Article Online
View Journal | View Issue

Cite this: *RSC Adv.*, 2025, **15**, 36642

Hydroperoxyl-bicarbonate mechanism for low-temperature CO oxidation by PdO/CeO_x/γ-Al_2O_3 mesoporous nanocatalysts

Anil C. Banerjee, *[ac] Isaac T. Olowookere,[b] Devon Cushing,[a] Santiago T. Salamanca,[b] Emily Knox,[a] Teriana Jackson,[a] Scott Bamonte,[b] Abiodun Aderibigbe,[b] Dilshan Silva[b] and Steven L. Suib *[bc]

Although substantial progress has been made in CO oxidation over supported noble metal catalysts, the development of an efficient Pd catalyst for complete CO oxidation below 150 °C still remains a challenge. In this study, a PdO/CeO_x/γ-Al_2O_3 catalyst synthesized by wetness and vortex methods showed excellent activity with a T_{50} of 80–90 °C and T_{100} of 120 °C. The catalyst had a large surface area of 150 m^2 g^{-1} and a pore diameter of 12 nm, which are characteristic of mesoporous materials. Pd(101), CeO_2(111) and γ-Al_2O_3 were identified by X-ray diffraction, high-resolution transmission electron microscopy (HRTEM) and X-ray photoelectron spectroscopy. HRTEM images showed PdO(101) nanoparticles (1–5 nm) dispersed over the mesoporous support. The high activity and stability of the fresh and spent catalysts may be due to the dispersion of PdO nanoparticles, the synergistic effect of support–support interactions, and the presence of defective oxygen and adsorbed water on the surface of catalysts and dual supports generating reactive oxygen species. Some of the unique features and advances reported in this study include the identification of PdO(101) as the active center for CO and O_2 activation, hydroperoxyl and bicarbonate intermediates, reduction of CO, mass transfer limitations (MTLs) at lower temperatures even when conversions are increasing, and high intrinsic activity of the catalyst overpowering MTLs. This study shows the potential of an efficient and stable PdO/CeOx/γ-Al_2O_3 catalyst for low-temperature CO oxidation under lean and dry conditions and the scope for further research on oxygen and CO activation.

Received 20th August 2025
Accepted 18th September 2025

DOI: 10.1039/d5ra06192j

rsc.li/rsc-advances

1. Introduction

Carbon monoxide (CO) is a colorless, odorless, flammable, and toxic gas that can persist in the air for extended periods. CO primarily originates from the incomplete combustion of gasoline, natural gas, and diesel fuels in automobiles, gas-powered generators, and flue gases from power plants, industrial processes and heating systems.[1,2] CO removal by thermal catalytic oxidation is considered the most energy-efficient method and is widely used in environmental pollution control, hydrogen fuel cells, CO sensors, and automotive exhaust systems. The development of catalysts for the complete removal of CO at low temperatures below 200 °C is particularly relevant for hydrogen and hydrocarbon fuel cells and catalytic converters in devices operating at lower temperatures. In recent decades, various catalysts, including noble metal catalysts, used for CO catalytic oxidation have been explored.[1–4]

Among the automotive catalysts, platinum and palladium metals on aluminum oxide[5–9] and cerium oxide[6,10–14] have been studied extensively for CO oxidation. However, comparatively, a limited number of research studies have been reported on the catalytic oxidation of CO by palladium catalysts on the dual support of aluminum oxide and cerium oxide.[15–20] The synthesis of Pd/ceria/alumina catalysts by flame spray pyrolysis, core–shell design, multistep sequential impregnation, multistep grafting, and incipient wetness with multiple pretreatments has been reported for CO oxidation.[15–20] The purpose of some of these advanced methods is to encapsulate/trap/anchor Pd particles with CeO_2 to improve stability and reduce deactivation,[16,18] but these methods may be difficult to scale-up for the production of catalysts. The conventional and simple method for the synthesis of Pd catalysts is wetness impregnation. The vortex method has been used in the industry to improve mixing through turbulence flow and generate nanoparticles,[21,22] but not for catalyst synthesis. A combination of wetness impregnation and vortex methods for the synthesis of nanocatalysts has been reported by our group.[23,24]

[a]*Department of Chemistry, Columbus State University, 4225 University Avenue, Columbus, GA 31907, USA*

[b]*Department of Chemistry, University of Connecticut, 55 North Eagleville Road, Storrs, CT 06269, USA. E-mail: steven.suib@uconn.edu*

[c]*Institute of Materials Science, University of Connecticut, 25 King Hill Road, Storrs, CT 06268, USA. E-mail: pdf25005@uconn.edu*

There is still a controversy about the active centers for O_2 and CO activation in the catalytic oxidation of carbon monoxide by Pd catalysts on a cerium oxide/aluminum oxide support. Several researchers reported PdO,[6,9,15,25–27] Pd^0,[5,16,17,19,20] or both PdO and Pd^0 [10,28–30] as the active centers for CO oxidation. The mechanism of CO oxidation and oxygen activation on noble metal catalysts has also been summarized in recent reviews.[1,31,32] CO oxidation by Pd and Pt catalysts on aluminum oxide generally follows Langmuir–Hinshelwood mechanism,[6,20,33] and on cerium oxide, it follows Mars-van-Krevelen mechanism.[6,26,34] Additionally, different reaction intermediates including formate, carbonate, peroxide, bicarbonate and hydroperoxyl have been reported in CO oxidation with Pd/CeO_2 and Pd/Al_2O_3.[11,17,35] However, the mechanism of CO oxidation and the identification of intermediate species by Pd catalysts on the dual support of cerium oxide and aluminum oxide have not been studied in detail.

Based on the knowledge gaps found from a comprehensive review of the literature, we designed a research study with the goals to develop a $PdO/CeO_x/\gamma\text{-}Al_2O_3$ catalyst, identify the active sites and reaction intermediates, and propose a reaction mechanism. In this study, we synthesized a $PdO/CeO_x/\gamma\text{-}Al_2O_3$ catalyst containing about 3 wt% Pd, 7 wt% CeO_2 and balance $\gamma\text{-}Al_2O_3$ (abbreviated as PdO/CA-fresh). The as-synthesized catalyst holds promise for low-temperature activity of CO oxidation to CO_2 at T_{50} of 85 °C, total conversion at 120 °C, and thermal stability at 500 °C. The catalyst contains about 80 wt% PdO and 20 wt% Pd as nanoparticles (1–5 nm) on the surface and dispersed over the mesoporous dual support of CeO_2 (111) and $\gamma\text{-}Al_2O_3$. Some of the unique observations and advances made in this study include identification of PdO(101) as the active centers for CO and O_2 activation and hydroperoxyl and bicarbonate as intermediates, reduction of PdO by CO, onset of mass transfer limitations (MTL) at lower temperatures even when conversion is increasing, and intrinsic activity of the catalyst overcoming the MTL.

2. Experimental section

2.1 Materials and reagents

Cerium nitrate hexahydrate (99.9%, crystalline), gamma-aluminum oxide ($\gamma\text{-}Al_2O_3$, 99.9%, crystalline, nanopowder, TEM particle size <50 nm, BET surface area = 40 $m^2\ g^{-1}$), and palladium nitrate dihydrate (about 40% Pd, crystalline) were purchased from Sigma-Aldrich.

2.2 Synthesis of catalysts and dual support

The cerium oxide/aluminum oxide dual support (CA) and PdO/CA fresh catalyst were synthesized by a combination of wetness impregnation and vortex methods.[23,24]

2.2.1. Cerium oxide-aluminum oxide dual support (CA). About 0.930 g of cerium nitrate hexahydrate was dissolved in 2.0 mL deionized water and transferred to an injection syringe in a syringe pump equipment (Fisher Scientific). A slurry of solid 4.70 g $\gamma\text{-}Al_2O_3$ (Sigma-Aldrich) pre-calcined at 500 °C was made with 20 mL deionized water in a vortex tube of a vortex apparatus (Fisher Scientific). The cerium nitrate solution was added at 20 μL min^{-1} to the vortex tube while being vortexed at 900 rpm for 5 h. The slurry was dried at 110 °C for 12 h and calcined at 500 °C for 5 h to obtain the dual support (CA).

2.2.2. Pd-fresh catalyst (PdO/CA-fresh). An aqueous solution of 0.24 g palladium nitrate dihydrate (Sigma-Aldrich) in 1.5 mL deionized water was added to about 3.0 g of the dual support in the vortex tube following the same procedure used for the synthesis of the dual support. The calcined sample was crushed and sieved to obtain a particle diameter of 38 μm. The as-synthesized catalyst was named 'PdO/CA-fresh'.

2.2.3. Pd-spent catalyst (PdO/CA-spent). The spent catalyst was prepared by treating the fresh catalyst with a 1% CO/4% O_2/N_2 gas mixture at 200 °C for 1 h in a fixed-bed-flow catalytic reactor.

2.3. Instrumental

Elemental analysis of Pd and Ce was performed by inductively coupled plasma-optical emission spectrometry (ICP-OES) using a PerkinElmer 5300 V spectrometer. The samples were prepared with sodium peroxide fusion due to the high content of Al_2O_3 followed by dissolution in water and acidification. The nitrogen sorption experiments were conducted using a Quantachrome Autosorb ASiQ-C instrument with nitrogen gas as the adsorbate at −196 °C in a multipoint method. The materials were first degassed at 150 °C for 6 h at a heating rate of 10 °C min^{-1} and under helium before the measurement. The surface areas were calculated by the Brunauer–Emmett–Teller (BET) method, and the pore sizes and distributions were calculated by the Barrett–Joyner–Halenda (BJH) method from the desorption data of the isotherm. CO temperature-programmed desorption (CO-TPD) experiments were conducted using Micromeritics Autochem II 2930 equipped with a TCD detector. About 0.05 g of the sample was treated in 10% CO/He for 60 min, followed by purging with He for 2 h. Then, the sample was heated up to 500 °C at a ramping rate of 10 °C min^{-1} under a flow of He (30 mL min^{-1}).

Powder X-ray diffraction (PXRD) patterns of the samples were collected at room temperature using a Rigaku Ultima IV instrument with Cu Kα (λ = 1.5406 Å) radiation at a beam voltage of 40 kV and a beam current of 44 mA. Wide-angle patterns were obtained by continuous scans at 2θ in the range of 10–85° at a scan rate of 2° min^{-1}. Solid-state nuclear magnetic resonance (NMR) spectra were recorded using a Bruker Avance III 400 WB with a 4 mm HXY probe tuned for ^{27}Al (104.2 MHz). The spinning frequency was kept at 7.5 kHz throughout the experiment. Aberration-corrected high-resolution transmission electron microscopy (AC-HRTEM), energy-dispersive X-ray spectroscopy (EDS) and high-angle annular dark-field scanning transmission electron microscopy (HAADF-STEM) measurements were conducted using a ThermoFisher Scientific Titan Themis S/TEM instrument. HRTEM images and elemental mapping were recorded using a Ceta camera and an EDS detector, respectively. The sample was dispersed on a carbon film in a Cu grid. X-ray photoelectron spectroscopy (XPS) data were recorded using a ThermoFisher K-Alpha X-ray photoelectron spectrometer with Al Kα radiation (λ

= 1486.6 eV). Each sample was applied to a double-sided carbon tape and secured on a sample holder. Charging was mitigated using an electron flood gun (0.0 V, 100 μA), an X-ray spot size of 400 μm, a take-off angle of 90°, and analyzer vacuum of at least 5.0×10^{-8} mbar before sample processing commenced. Pass energies were 200 and 50 eV for the survey and core scans, respectively. Energy step sizes were 1.0 and 0.1 eV for the survey and core scans, respectively. The dwell time was 50 ms. Peak fittings were done using the CasaXPS software (v. 2.3.25 PR 1.0) and charge correction was done with reference to C 1s photoelectron line (284.8 eV).

The diffuse reflectance infrared Fourier-transform spectroscopy (DRIFTS) measurements were conducted in a Harrick praying mantis cell using a Nicolet 6700 IR spectrometer. A liquid nitrogen-cooled MCT detector was used, and the spectra were recorded over 256 scans with a resolution of 4 cm^{-1}. About 50 mg of a sample was put in a holder cup in a gas cell and flushed with nitrogen at 150 °C. The gas cell was then cooled to 25 °C using a ThermoScientific Thermoflex 900 Chiller, and 25 SCCM (standard cm^3 min^{-1}) of 10% CO in balance N_2 was passed over the sample in the gas cell to equilibrate for 15 min and then the CO/N_2 gas flow stopped. The absorbance was recorded and Omnic software was used for data acquisition and processing. This was followed by flushing the gas cell with 25 SCCM N_2 for 5 min to remove physiosorbed gases and the DRIFTS spectra were recorded again. The *in situ* DRIFTS experiments were conducted in the same Harrick cell using a fresh sample, and degassing in argon at 150 °C. The cell was cooled to 40 °C, 25 SCCM of 1% CO/4% O_2/N_2 was introduced into the cell for 15 min to equilibrate, and then a spectrum was recorded. The procedure was repeated at 60–200 °C. For the *in situ* DRIFTS spectra with the reduced PdOCA catalyst, the fresh sample was reduced *in situ* with 5% H_2/N_2 for 1 h at 400 °C, followed by *in situ* drifts measurements in the presence of 1% CO/4% O_2/N_2.

2.4. Catalytic test for CO oxidation

The CO oxidation activity measurements were conducted in a fixed-bed quartz tube reactor inserted in a temperature-controlled horizontal tubular furnace (Carbolite, Verder Scientific). The temperature of the catalyst bed was increased to a fixed value under a flow of N_2 followed by the flow of the reacting gas mixture (1 vol% CO, 4 vol% O_2, N_2 balance) at a flow rate of 150 cm^3 min^{-1} for 1 h. After the reaction time, a sample of 1.0 cm^3 of the gas mixture from the reactor outlet was collected in a Luer-Lock gas-tight syringe (Restek) and injected into a gas chromatograph (SRIGC 310) fitted with a 'Shin carbon' packed column (Restek) and a thermal conductivity detector. The CO conversion (% v/v) was calculated as: $(CO_{inlet} - CO_{outlet})/CO_{inlet} \times 100\%$, where CO_{inlet} and CO_{outlet} are the inlet and outlet CO concentrations (vol%) at 25 °C and 1.0 atm in the gas mixture before and after the reaction.

For the determination of activation energy and reaction rates, the activity measurements were conducted in the kinetic region with CO conversion below 15%. The activation energy was calculated from the Arrhenius plot. The time and temperature stability as well as the reusability tests with the fresh and spent catalysts were conducted in a catalytic reactor. The activity and stability experiments were conducted under steady-state conditions with a gas hourly space velocity (GHSV) of 90 000 (cc g_{cat}^{-1} h^{-1}). Each experiment was repeated three times, and the average value was accepted if the error was within 5%.

3. Results and discussion

3.1. Synthesis and characterization

3.1.1. Synthesis and elemental composition of the as-synthesized catalysts and dual support. The conventional wetness impregnation method was modified by adding a vortex mixer for uniform mixing of the components.[23,24] The catalytic activity of Pd/cerium oxide/aluminum oxide catalysts depends on Pd and Ce loadings. We initially synthesized a $PdO/CeO_x/\gamma$-Al_2O_3 catalyst with 1 wt% Pd loading and could not detect Pd components by AC-HRTEM and PXRD due to high dispersion of Pd nanoparticles in the support.[17] Hence, we chose a higher Pd loading of 3 wt%.[36] Similarly, about 6 wt% cerium oxide was selected based on reported studies on optimum cerium oxide content for better activity in CO oxidation.[15]

The elemental compositions of Pd and Ce in the $PdO/CeO_x/\gamma$-Al_2O_3 fresh (PdO/CA-fresh) and $PdO/CeO_x/\gamma$-Al_2O_3 spent (PdO/CA-spent) catalysts are given in Table S1. Both catalysts contain about 3 wt% Pd and 6 wt% Ce and the experimental and calculated values are similar, indicating atom economy in the synthesis of the catalysts. About 6 wt% Ce is present in the dual support CeO_x/γ-Al_2O_3 (CA) as per stoichiometric calculation used for the synthesis.

3.1.2. Morphological studies of the as-synthesized catalysts and dual support. The textural properties of the fresh and spent catalysts and dual support were evaluated by conducting an N_2 adsorption–desorption experiment. The physicochemical properties are displayed in Fig. 1 and Table 1. All the samples exhibit a type IV isotherm (Fig. 1a) traditionally associated with mesoporous materials.[4,34,37] The pore size distributions (Fig. 1b) show a broad peak centered around 12 nm for the fresh and spent catalysts. The pore size and pore volume of the dual support are comparable to those in the catalysts. The pore volume and pore diameter of the reference γ-Al_2O_3 are higher, and the values decrease in the catalysts and dual support likely due to the shrinkage of the pores during the synthesis of the support and calcination at 500 °C.[38] The BET surface areas of the as-synthesized catalysts and the dual support are 150–158 m^2 g^{-1} (Table 1).[5,15,16] Based on the BET surface areas and nanosized pore diameters (11–14 nm), the catalysts and the dual support are categorized as mesoporous materials.[34,37,39]

The HAADF-EDS images (Fig. 2 and S1) of the fresh and spent catalyst samples show small PdO nanoparticles (about 2–5 nm) dispersed on the cerium oxide and aluminum oxide support[6,15,25–27] Some PdO crystallites are near the cerium oxide crystallites but there is no evidence of anchoring/trapping/encapsulation by cerium oxide contrary to previous reports.[15–17] The cerium oxide nanoparticles are spread over

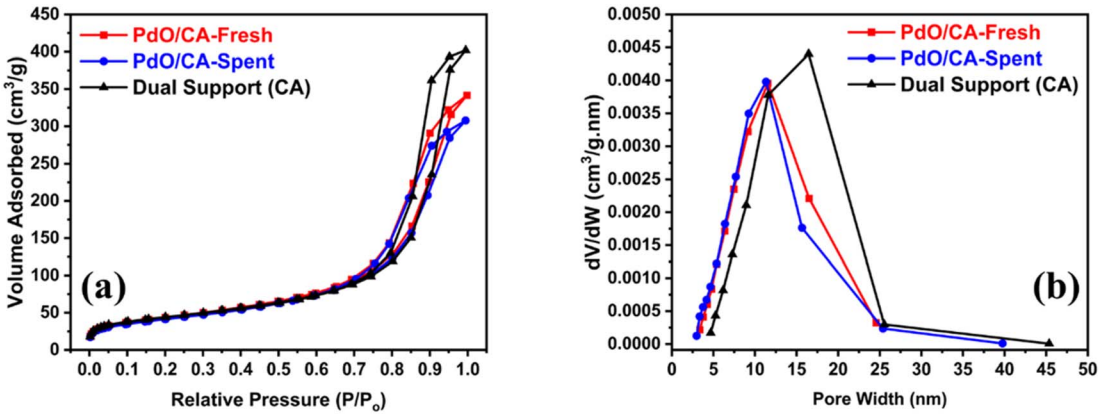

Fig. 1 (a) N_2-sorption isotherm and (b) BJH desorption pore size distribution of the as-synthesized catalyst samples.

Table 1 Physicochemical properties of the as-synthesized catalyst and support

Catalyst/support	PdO crystallite size (nm)[a]	BET surface area ($m^2\ g^{-1}$)	BJH pore volume ($cc\ g^{-1}$)	BJH pore diameter (nm)
PdO/CA-fresh	2.8	158	0.50	11.5
PdO/CA-spent	2.4	150	0.48	11.3
Dual support (CA)	—	157	0.62	13.8
γ-Al_2O_3[b]	—	170	1.2	21.3

[a] AC-HRTEM. [b] Sigma-Aldrich.

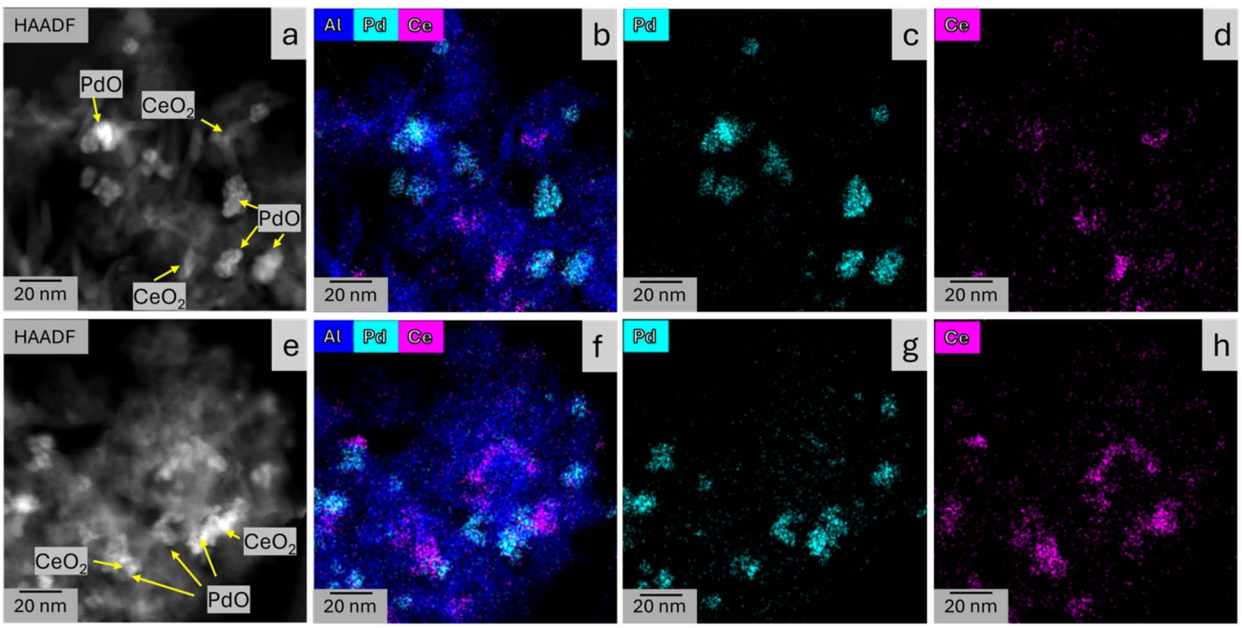

Fig. 2 (a–d) HAADF and EDS elemental mappings of PdO/CA-fresh catalyst and (e–h) HAADF and EDS elemental mappings of PdOCA-spent catalysts.

gamma-aluminum oxide and some cerium oxide particles form clusters (Fig. 2 and S1).[15–17]

To obtain the shapes and sizes of PdO and cerium oxide particles, AC-HRTEM 50 nm Ceta images of the fresh and spent catalysts were collected and analyzed. Fig. 3a, b, d and e show pebble-like and rod-like shapes of cerium oxide in the fresh and spent catalysts, which are characteristics of the exposed CeO_2(101) facets. The crystal planes and the lattice fringes for PdO(101) and CeO_2 are shown in the AC- HRTEM 5 nm Ceta images (Fig. 3c, f and S2). Interplanar spacings (*d*-spacings)

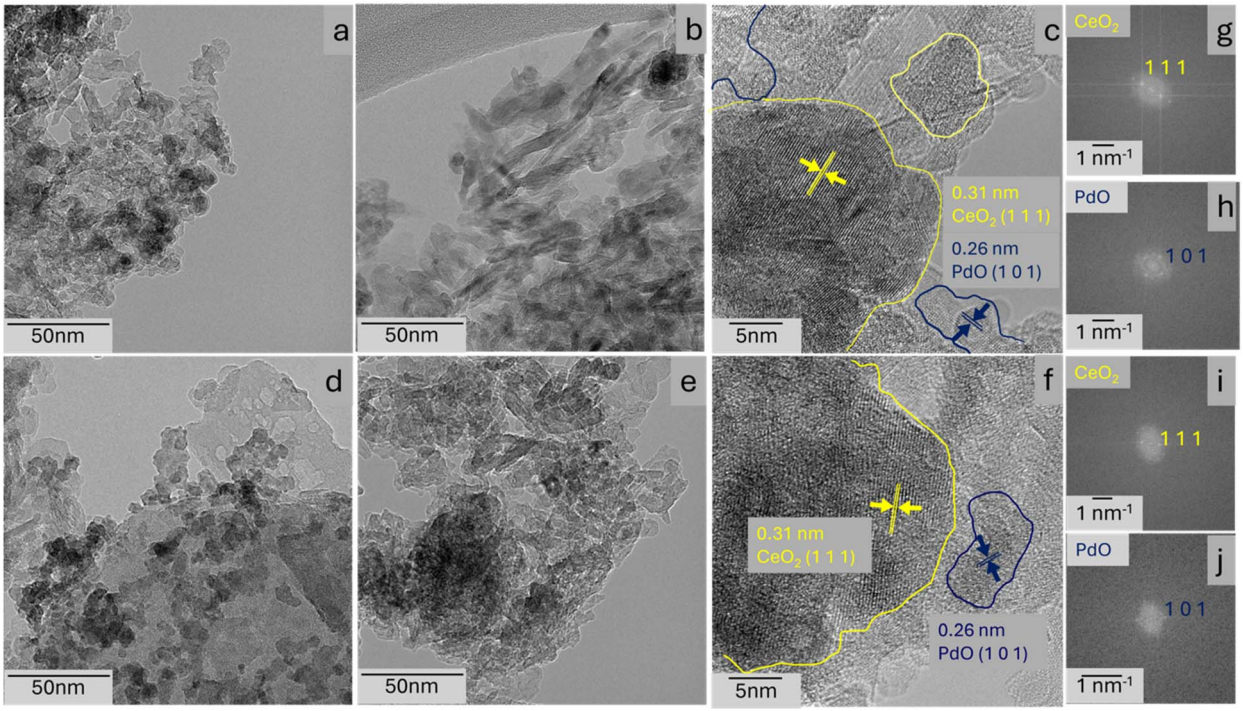

Fig. 3 HRTEM Ceta images of PdO/CA-fresh (a–c) and PdO/CA-spent (d–f) catalysts, displaying their morphologies: (c and f) lattice fringes and crystal planes in the crystallites of PdO and CeO_2 in 5 nm Ceta HRTEM images; (g–j) FFT patterns of (c and f).

were determined using the ImageJ software (version 1.54p) by generating Fast Fourier Transform (FFT) images from high-resolution transmission electron microscopy (HRTEM) micrographs. The *d*-spacing values (Fig. 3c and f) were calculated by measuring the distance between pairs of opposite diffraction spots in the FFT patterns (Fig. 3g–j), providing a reliable estimation of lattice parameters.[40] The lattice fringes measuring 0.26 nm can be ascribed to PdO(101) based on the International Center for Diffraction Data (ICDD) given in Table S2. Similarly, the lattice fringe of 0.31 nm is attributed to CeO_2(111) based on the ICDD (Table S2). Additionally, Fig. S2 also shows the crystal lattices measuring 0.19 nm, which can be assigned to the CeO_2(220) crystal facets (Table S2), and these crystal facets are more exposed in the spent catalyst sample. The lattice fringes in the PdO(101) crystallites with clear boundaries and shapes were counted to determine the average crystallite size of PdO in the fresh and spent catalysts. The average PdO crystallite sizes of fresh and spent catalysts are 2.8 nm and 2.4 nm, respectively (Table 1). The HAADF and HRTEM images of the dual support (Fig. S3 and S4) show rod-like structures of cerium oxide.

3.1.3. Chemical states and composition of the as-synthesized catalysts and dual support. The powder X-ray diffraction (PXRD) patterns of fresh and spent catalysts, dual support and reference standards are shown in Fig. S5a. The XRD data from the International Center for Diffraction Data (ICDD) for PdO, Pd^0, CeO_2, Ce_2O_3, and γ-Al_2O_3 are given in Table S2. The PdO/CA fresh and spent catalysts show four major 2-theta peaks at 28.7°, 33.7°, 45.5°and 67°. The 28.7° peak is assigned to CeO_2(111), and the peaks at 45.5° and 67°are assigned to γ-Al_2O_3. The peaks that are close to 33.7° are of PdO(101) or CeO_2(200). The dual-support CeO_2/γ-Al_2O_3 shows a peak at 33.7° but the peak intensity is lower than that in the PdO/CA fresh and spent catalysts. Therefore, the peak at 33.7° cannot be ascribed to CeO_2 since the content of CeO_2 is the same (about 7%) in the support and the catalysts. Therefore, the peak at 33.7° is assigned to PdO(101). This facet of PdO is also detected in the HRTEM images in the fresh and spent catalysts (Fig. 3). The major 2-theta peaks of the dual support at 28.7°, 45.5° and 67° confirm the presence of CeO_2(111) and γ-Al_2O_3. In short, the presence of PdO(101) is confirmed by XRD, but no Pd^0, indicating high dispersion of metallic Pd in the catalysts.[6,25,27,36]

Solid-state ^{27}Al nuclear magnetic resonance (NMR) spectroscopic measurements were conducted to identify the coordination numbers of Al in the catalysts and dual support (Fig. S5b). Typically, in the ^{27}Al NMR spectra, a six-coordinate peak appears at *ca.* 0–20 ppm, five coordinated peaks at *ca.* 30–50 ppm, and four coordinated (tetrahedral) peaks at *ca.* 50–80 ppm. The results indicate that the as-synthesized catalyst samples and the dual support have six- and four-coordinated Al^{3+} sites.[41]

The chemical states of Pd, Ce, and O in the fresh and spent catalysts were investigated by means of X-ray photoelectron spectroscopy (XPS), and the results are shown in Fig. 4 and Table S3. The XPS fitting parameters for Pd 3d and Ce 3d are tabulated in Tables S4 and S5. The Pd 3d spectra were recorded with 5 scans each because the catalysts are suspected to contain PdO, which is rapidly reduced to Pd^0 by the X-ray beam. This explains the lower signal-to-noise ratio in the Pd 3d spectra in comparison to the Ce 3d spectra. The curve fitted Pd $3d_{3/2}$ and Pd $3d_{5/2}$ core spectra (Fig. 4a) show high-intensity peaks with

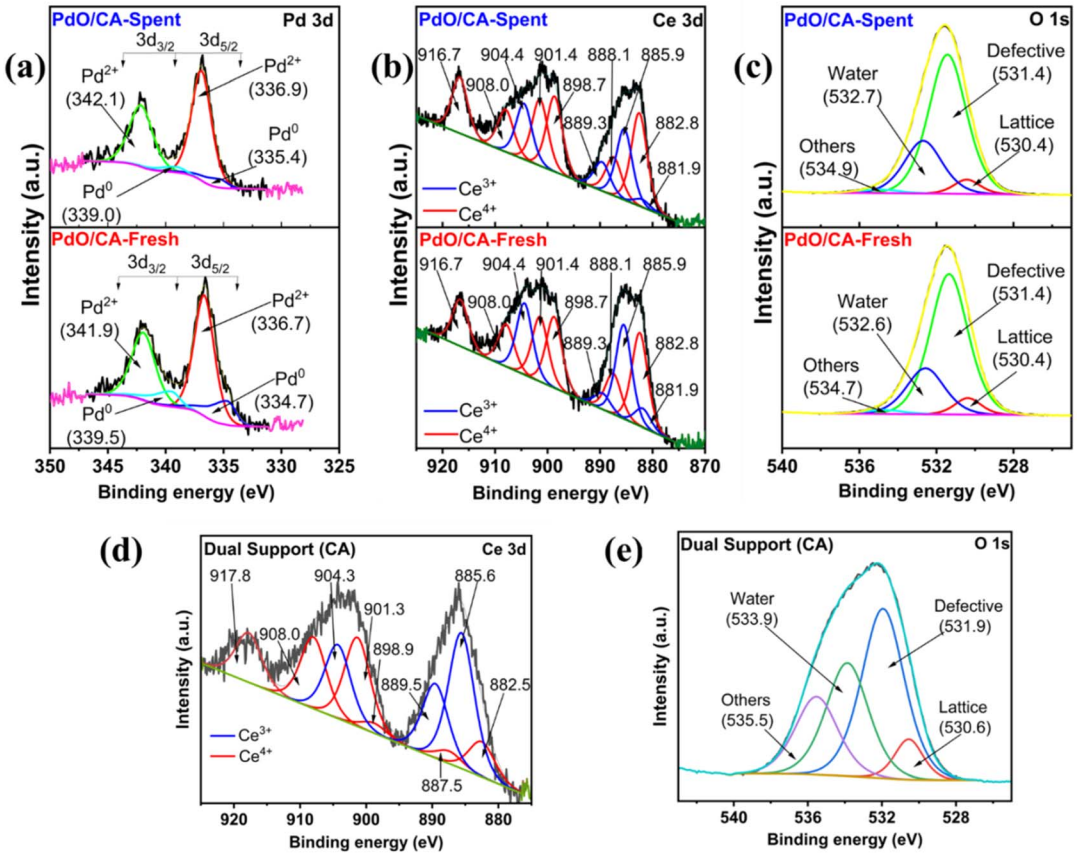

Fig. 4 Curve fitted (a) Pd 3d, (b) Ce 3d, and (c) O 1s X-ray core level spectra for the catalyst samples and (d) Ce 3d and (e) O 1s for the support.

binding energies of about 342 and 337 eV corresponding to Pd^{+2}. Further, the XPS spectra also show two low-intensity peaks at about 339 and 335 eV corresponding to the binding energies of Pd^0. Based on the deconvolution of the XPS peaks, the contents of Pd^0 and Pd^{+2} were calculated as 21% and 79%, respectively, in the fresh catalyst, and 10% and 90%, respectively, in the spent catalyst. The results confirm that Pd is present mainly in the oxidized state in both fresh and spent catalysts.[15,25,27,36]

The XPS data for the Ce oxidation states in the catalyst samples and dual support are given in Fig. 4b and d. The Ce 3d core scans contain both Ce^{3+} and Ce^{4+} states (Fig. 4b). The peaks at 881.8, 885.7, 888.8, and 904.4 eV belong to Ce^{3+}. All other peaks in the Ce 3d spectra represent Ce^{4+}, among which the peak at 916.5 eV is unique to Ce^{4+}. The data for the dual support is similar. The XPS data in Fig. 4 and Table S3 confirm the presence of Ce^{+3} and Ce^{+4} oxidation states in both catalysts and dual support.[16,25,26,42] The dual support contains about 44% Ce^{+3} and 56% Ce^{+4}. It seems only part of Ce^{+3} is present in the precursor, and cerium(III) nitrate got oxidized to Ce^{+4} state during calcination in air at 500 °C, indicating incomplete oxidation during the calcination process in the synthesis of the dual support.[43–45]

The curve fitted oxygen core scans show the presence of surface oxygen species as defective oxygen (V_O^x, 68–70%) and adsorbed water (23–26%) in the fresh and spent catalysts (Fig. 4c, e, Tables S3 and S6).[17] The dual support also has oxygen species with 44% defective oxygen, 29% water and 20% others.[45]

3.1.4. PdO–support interactions (temperature-programmed desorption). The PdO-cerium oxide interfaces in the 5 nm Ceta AC-HRTEM images (Fig. S2) indicate interactions between CeO_2 and PdO through Pd–O–Ce bonds even though no anchoring of PdO by CeO_2 is observed in the PdO/CA fresh and spent catalysts.[15,17,25,27,36] The temperature-programmed CO desorption of the PdO/CA-fresh catalyst and dual support profile is shown in Fig. S6. The first peak at about 100 °C indicates CO desorption from cerium oxide in the support and CO adsorbed on PdO(101).[20] The desorption peak at 325 °C indicates that CO could remain adsorbed on ceria at higher temperatures.

3.2. Catalytic properties of $PdO/CeO_x/\gamma\text{-}Al_2O_3$

3.2.1. Activity and stability of the catalysts. The catalytic activity of the PdO/CA fresh and spent catalysts is shown in Fig. 5a. The PdO/CA-fresh catalyst shows excellent low-temperature activity for CO oxidation with T_{50} and T_{90} at 80 °C and 110 °C, respectively (Fig. 5a). The initial rate and apparent activation energy for CO oxidation with the fresh catalyst are 0.045 CO mmol g_{Pd}^{-1} s^{-1} (4.6 CO mmol g_{cat}^{-1} h^{-1}) and 61.7 kJ mol^{-1}, respectively (Fig. 5c and Table S7). Similar Pd/CA catalysts prepared by a conventional wetness impregnation

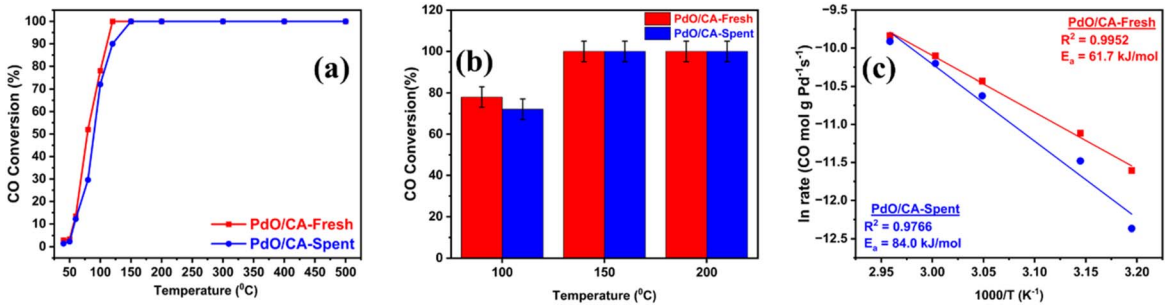

Fig. 5 (a) Light-off temperature, (b) comparative activities at three temperatures, and (c) activation energy of PdO/CA-fresh and PdO/CA-spent catalysts for CO oxidation. Conditions: GHSV 90 000 (cc g_{cat}^{-1} h^{-1}); 1 h reaction time at each temperature to reach a steady state.

method showed lower CO oxidation activity with T_{50} at 130–210 °C and T_{90} at 150–240 °C.[16,17,37] PdO/CA catalysts synthesized by flame spray pyrolysis, core shell design and two-step incipient impregnation methods also exhibited higher T_{50} at 90–210 °C and T_{90} at 130–220 °C in comparison to the PdO/CA fresh catalyst results reported in this study.[15–17] The activity of Pd/aluminum oxide catalysts prepared by a wetness impregnation method also exhibited higher T_{50} at 140–260 °C and T_{90} at 160–270 °C in comparison to the PdO/CA fresh catalyst results reported in this study.[5,6,8,9] Similar Pd/cerium oxide catalysts also exhibited higher T_{50} at 90–130 °C and T_{90} at 140–350 °C.[6,10,35] However, the $Pd/CeO_2/Al_2O_3$, Pd/Al_2O_3 and Pd/CeO_2 catalysts referenced here may have different Pd loadings compared to the PdO/CA catalyst used in this study. Hence, the comparison of activities is in general.

The spent catalyst (PdO/CA-spent) obtained after reacting the fresh PdO/CA catalyst with 1% CO/4% O_2/N_2 at 200 °C for1 h also shows excellent low temperature activity and initial rate comparable with the fresh catalyst (Fig. 5a, Table S7), but a higher activation energy (Fig. 5c). Additionally, both the fresh and spent catalysts show high CO activity with 70–80% conversion at 80 °C and 100% conversion at 150 °C and 200 °C (Fig. 5b). The initial rate with both catalysts increases significantly when the temperature is increased from 50 °C to 60 °C, indicating CO oxidation reaction at a lower temperature range controlled by the Arrhenius activation theory (Table S9). The results in Fig. 6a and b show that both the fresh and spent catalysts have high time (42 h) and temperature stability (200–500 °C) under the experimental conditions of high CO conversions >98%. Additionally, the results in Fig. 6c with 98–100% CO conversion after three cycles confirm the stability and durability of the catalyst over long-term use (12 h) during CO oxidation. The heating and cooling catalytic cycles (Fig. S7) for the fresh catalyst show the absence of hysteresis[36,39] between ignition temperature (30 °C) and extinction temperature (25 °C). The dual support does not show any CO conversion at lower temperatures up to 200 °C but is active at a higher temperature of 500 °C with 50% CO conversion (Table S8).

Based on the electron affinity values of Pd, Ce and Al and the oxygen storage capacity of cerium oxide, it is expected that Pd/CeO_2 catalysts would exhibit strong Pd–Ce interfaces and better activities compared to Pd/Al_2O_3 and $Pd/CeO_2/Al_2O_3$ catalysts. However, in our study, the Pd–Ce interfaces and interactions are not prominent and in clear contradiction to studies reported previously.[15,17,25,36,46] The excellent low-temperature catalytic activity of the PdO/CA fresh and spent catalysts is likely due to the presence of small PdO nanoparticles dispersed over the mesoporous support with high surface and high intrinsic activities. The high activity and stability of the fresh and spent catalysts may also be due to the synergistic effect of support–support interactions between gamma aluminum oxide and cerium oxide[44,45] and the presence of defective oxygen, adsorbed

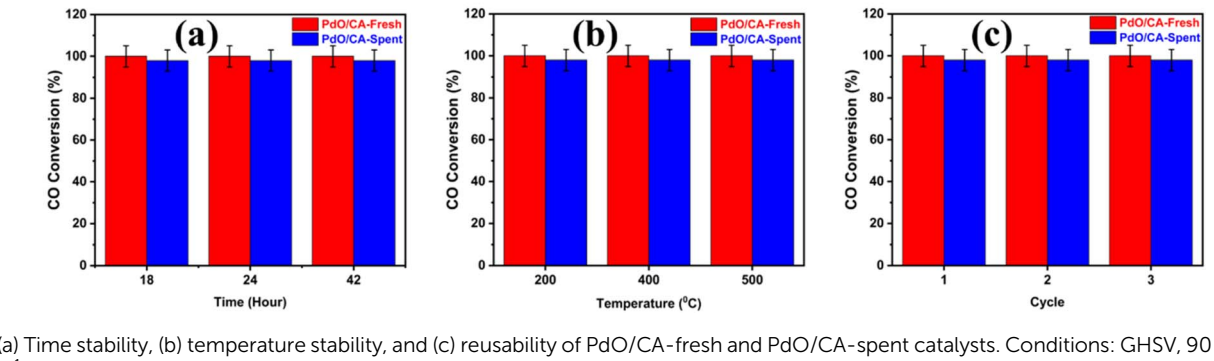

Fig. 6 (a) Time stability, (b) temperature stability, and (c) reusability of PdO/CA-fresh and PdO/CA-spent catalysts. Conditions: GHSV, 90 000 (cc g_{cat}^{-1} h^{-1}) for all: (a) reaction temperature = 200 °C; (b) 1 h reaction time at each temperature; and (c) reaction temperature = 200 °C, 4 h reaction time for each cycle.

water/hydroxyl group on the surface of the catalysts and dual support generating reactive oxygen species.[11,17,38]

3.2.2. Mass transfer limitations (MTLs). The presence of MTL at 50–200 °C was determined using the Weisz-Prater criteria (C_{w-p}) and Mears' criteria (M_{ext}) for internal and external mass transfer limitations, respectively.[47,48]

$C_{w-p} > 1$ and $M_{ext} > 0.15$ indicate the presence of internal mass transfer limitations and external mass transfer limitations, respectively. The data for MTL calculations based on the Weisz-Prater and Mears' criteria are given in Table S9 followed by MTL calculations with the data at 60 °C as an example. Table S10 gives the values of C_{w-p} and M_{ext} for PdO/CA-fresh and PdO/CA-spent catalysts at 50–200 °C. For MTL calculations, the relative magnitudes of the robs (rate) and De (Knudsen diffusivity) are critical, and both these factors are temperature dependent. At 60 °C, when catalyst conversion is 12–13%, the rate is low and kinetically controlled, and hence no MTL. The value of $C_{w-p} > 1$ at 80–200 °C indicates the onset of MTL due to internal mass diffusion even at a low temperature of 80 °C with CO conversion of 52.0% and 29.6% for the fresh and spent catalysts, respectively. This is rather unusual for a powdered catalyst of particle diameter 38 μm and activity measured at a low temperature of 80 °C. The M_{ext} values are less than 0.15 in all cases, indicating no MTL due to external mass transfer. This is expected since the activity measurements are done with a small particle size of 38 μm and a high GHSV of 90 (L g_{cat}^{-1} h^{-1}).

We have included mass transfer limitations (MTL) in this study even though it is normally assumed that CO oxidation would be under kinetic control at lower temperatures below 200 °C. However, very strangely, the Weitz-Prater (C_{w-p}) value comes greater than 1 even at a low temperature of 80 °C. If the internal diffusional resistance is controlling, then the kinetics should get hampered, which is not the case here. The catalysts seem to have high intrinsic catalytic activity independent of MTL as indicated by high conversion at low temperatures and the intrinsic activity may overcome the mass transfer limitations due to internal diffusion.

3.3. Investigation of reaction mechanism

3.3.1. Identification of adsorbed and intermediate species by diffuse reflectance infrared Fourier transform spectroscopy (DRIFTS) studies. The *ex situ* DRIFTS CO adsorption experiments (Fig. 7a and b) show two unique CO-adsorption peaks at 2094 cm^{-1} and 2133 cm^{-1}. The 2094 cm^{-1} peak is assigned to adsorbed CO on PdO(111) and the peak at 2133 cm^{-1} is assigned to CO adsorbed on PdO_2 species.[25,26] The peak at 2360 cm^{-1} is assigned to CO_2 (*g*) formed by reduction of PdO by CO during CO adsorption.[9,15,25]

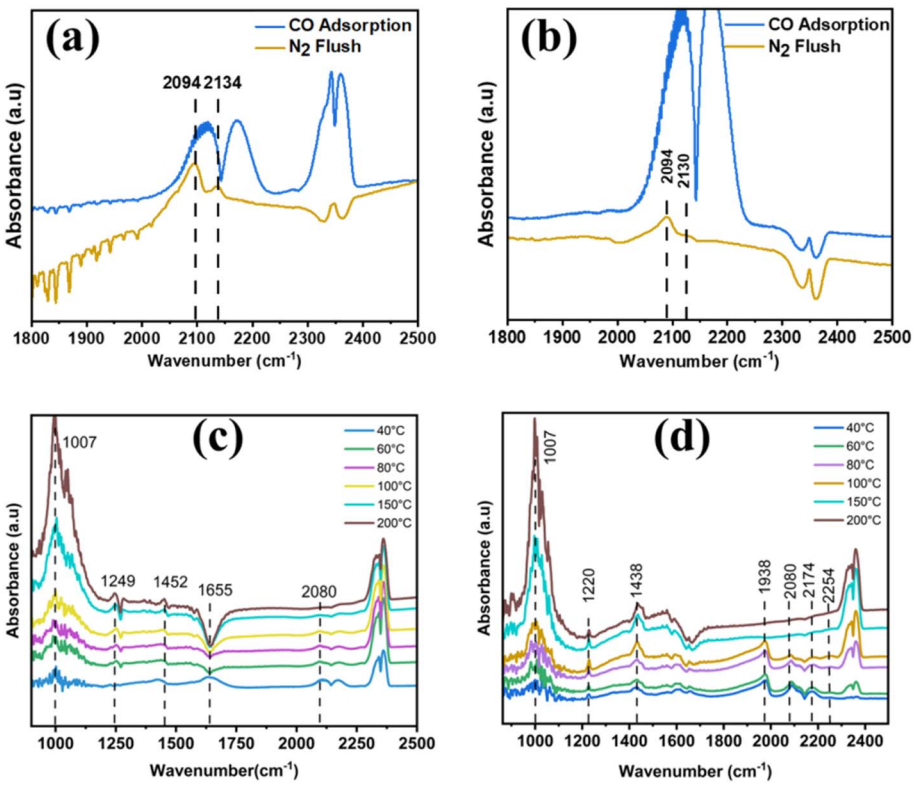

Fig. 7 CO adsorption DRIFTS of (a) PdO/CA-fresh and (b) PdO/CA-spent. *In situ* DRIFTS with 1% CO/4% O_2/N_2 of (c) PdO/CA-fresh and (d) PdO/CA-reduced. CO adsorption DRIFTS spectra were collected after flow of 20 SCCM CO and flushing with 20 SCCM of N_2. For *in situ* DRIFTS measurement, 25 SCCM of 1% CO/4% O_2/N_2 was introduced into the gas cell for 15 min to equilibrate, and then, a spectrum was recorded. The procedure was repeated at 40–200 °C. For the *in situ* DRIFTS spectra with the PdO/CA-reduced catalyst, the fresh sample was reduced *in situ* with 5% H_2/N_2 for 1 h at 400 °C, followed by *in situ* drifts measurements in the presence of 1% CO/4% O_2/N_2.

To explore the mechanism of CO oxidation in the presence of oxygen, we examined the *in situ* DRIFTS data of the as-synthesized fresh and reduced PdO/CA catalysts (Fig. 7c and d). The band at 2080 cm^{-1} is due to linearly adsorbed CO on PdO(101).[15,25] In the PdO/CA fresh catalyst, the bands at 1850–1950 cm^{-1} usually assigned to linear and bridged Pd–CO bonds are not clear, but these bands reappear in the reduced catalyst, suggesting CO adsorption on larger crystallites of reduced PdO.[15,17,25] The bands 2240 cm^{-1} and 2350 cm^{-1} are assigned to Al binding to carbon monoxide[15] and CO_2 (g),[15,25] respectively.

To identify the adsorbed oxygen and carbon species on the surface of the fresh and reduced catalysts, the IR bands in the 800–1750 cm^{-1} regions are analyzed. The band at1007 cm^{-1} is attributed to a hydroperoxyl intermediate (*OOH).[17,49] Both the fresh and reduced catalysts show a bicarbonate intermediate at about 1240 cm^{-1}.[11,17] The peak at 1660 cm^{-1} is typically assigned to OH stretching of water, hinting that hydroxyl groups are involved in the CO oxidation reaction.[17,38] The peak intensities for *OOH and CO_2 (g) increase with temperature, indicating the participation of the *OOH group in the CO oxidation at higher temperatures. The DRIFTS data for the reduced catalyst (Fig. 7d) also show the IR peaks for the hydroperoxyl (1000 cm^{-1}) and bicarbonate (1220 cm^{-1}) intermediates.

To investigate whether oxygen activation could also happen on the dual support of CeO_x and γ-aluminum oxide (CA), we performed the *in situ* DRIFTS measurements with the cerium oxide/aluminum oxide support in the presence of oxygen (Fig. 8). The results show hydroperoxyl intermediate at *ca.* 1000 cm^{-1}, and several weak peaks were assigned to adsorbed bicarbonates (1280 cm^{-1}), carbonates (1450 cm^{-1}), adsorbed water (1650 cm^{-1}), CO–Al (2180 cm^{-1}), and CO_2 (2350 cm^{-1}).

3.3.2. Reaction mechanism. Based on the experimental and inferential evidence, we propose two schemes (Scheme 1 and 2) for oxygen and CO activation in the CO oxidation reaction following the hydroperoxyl-bicarbonate pathway. Scheme 1 follows the O_2 and CO activation on electron-deficient PdO sites produced by reduction of PdO by CO during CO oxidation. The IR band at 1007 cm^{-1} (Fig. 7c and d) is attributed to a hydroperoxyl intermediate (*OOH).[17,49] The O 1s XPS data (Fig. 4 and Table S3) show high percentages of defective oxygen (V_O^x) and adsorbed water in the catalyst samples and support.[17] The hydroperoxyl group is likely formed by the protonation of O_2 adsorbed on a partly reduced electron-deficient PdO site by adsorbed H_2O from a neighboring cerium oxide/aluminum oxide site.[17] Both the fresh and reduced catalysts show a bicarbonate intermediate (Fig. 4c and d) at about 1240 cm^{-1}.[11,17] The bicarbonate intermediate is likely formed by the transfer of the hydroperoxyl group to the adsorbed CO on an adjacent Pd site.[11,17]

Scheme 2 is based on oxygen activation on the support through oxygen adsorption and protonation on the support sites to form a hydroperoxyl intermediate and then transfer of the intermediate to CO adsorbed on the electron–deficient PdO site to form a bicarbonate intermediate. The detection of hydroperoxyl intermediate on the dual support indicates the possibility of oxygen adsorption and subsequent protonation by absorbed water on the surface of the support.

Both schemes are related to the Langmuir Hinshelwood mechanism with the PdO sites,[6,15,25,27] likely the active centers for CO and O_2 activation and the dual support for O_2 activation.[43–45,50]

CO oxidation on a PdO/CA catalyst may also follow a Mars-van-Krevelen (MvK) mechanism involving lattice or defective oxygen on the surface.[6,26,34] The CO adsorption DRIFTS measurements in the absence of oxygen (Fig. 7a and b) show the formation of CO_2 gas indicating the possibility of participation of lattice oxygen. However, the low intensity of the CO_2 peak after nitrogen flash indicates negligible contribution from lattice oxygen. This result is further verified by no CO conversion to CO_2 in a reaction of the PdO/CA -fresh catalyst with 1% CO/N_2 at 200 °C for 1 h. The CO oxidation by the CeO_x/Al_2O_3 support is also negligible at 200 °C (Table S8), suggesting that lattice oxygen from cerium oxide or aluminum oxide may not be contributing in a significant way to the CO oxidation through the MvK mechanism.

Several alternative reactive oxygen species and intermediates have also been identified for CO oxidation by Pd/CeO_2 catalysts, including carbonates and formates,[11] peroxides,[35] and superoxides, and peroxides for Au/CeO_2 catalysts.[51] Kim, Lee and Kwak[35] performed density functional theory (DFT) calculations and revealed the formation of a unique zigzag chain structure by the oxygen and Ce atoms of the topmost surface of CeO_2(100) with Pd atoms located between the zigzag chains and identified the adsorbed oxygen species as peroxides using *in situ* Raman spectroscopy. Liu *et al.*[46] proposed three different reaction mechanisms for CO oxidation on Pd nanorod/CeO_2(111) based on density functional theory (DFT) calculations. The adsorbed O_2 species at the Pd–Ce^{+3} interface, the lattice oxygen at the interface, and the adsorbed O_2 species on the Pd nanorod were proposed as the active species in these three mechanisms, respectively, and concluded that the dominant reaction pathway for CO oxidation at low temperatures was the Pd–Ce^{+3} dual-site mechanism.

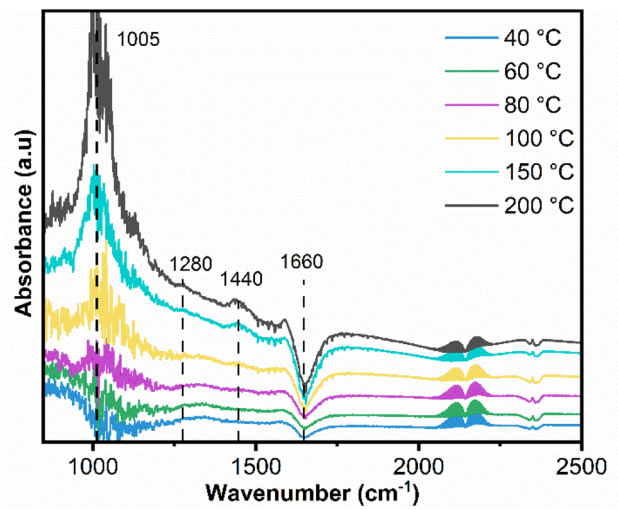

Fig. 8 *In situ* DRIFTS spectra of the dual support (CeO_x/Al_2O_3). The *in situ* DRIFTS experiment was conducted in the gas cell by degassing in argon at 150 °C and cooling to 40 °C; 25 SCCM of 1% CO/4% O_2/N_2 was introduced into the cell for 15 min to equilibrate, and then, a spectrum was recorded. The procedure was repeated at 40–200 °C.

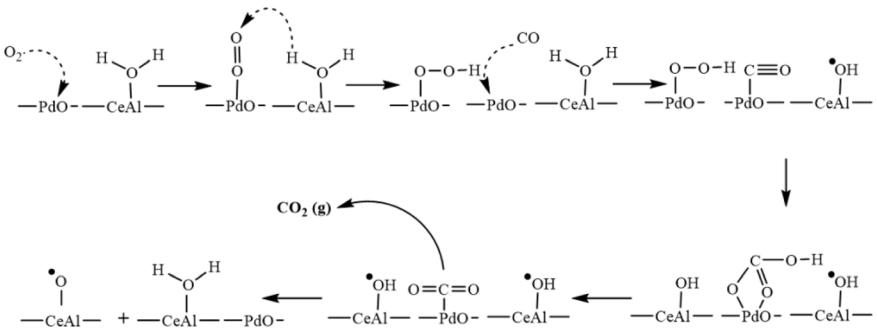

Scheme 1 Mechanism of CO oxidation through O_2 activation on Pd and transfer of the hydroperoxyl intermediate to CO adsorbed on Pd.

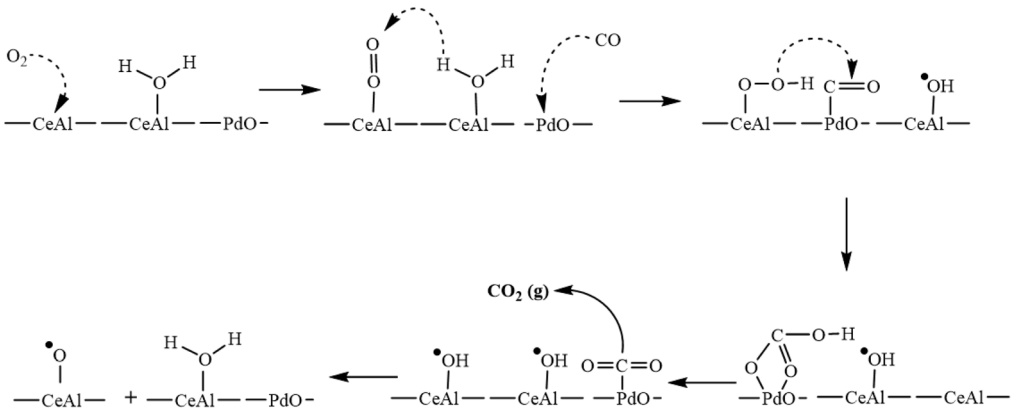

Scheme 2 Mechanism of CO oxidation through O_2 adsorption on the ceria/alumina support and transfer of the hydroperoxyl intermediate to CO adsorbed on Pd.

The high amount of defective oxygen and adsorbed water in the dual support and the oxygen storage capacity of cerium oxides may generate reactive oxygen species (ROS). The detection of hydroperoxyl intermediates in the *in situ* DRIFTS measurements is a unique part of this study since only a few previous studies reported this intermediate in CO oxidation by $Pd/CeO_x/Al_2O_3$ and Pd/CeO_2 catalysts.[17] The dual support with plenty of ROS may facilitate the formation of the hydroperoxyl and bicarbonate intermediates as pathways for CO oxidation following the Langmuir–Hinshelwood mechanism with oxygen adsorption on PdO or the dual support. *In situ* DRIFTS data (Fig. 7 and 8) indicate the presence of CO–Al bonds and the possibility of oxygen activation on the gamma-alumina sites. The FTIR studies on oxygen adsorption on CeO_2 stabilized by superoxide species (O_2^-) at 1130 cm^{-1},[50] bicarbonates (1220 cm^{-1}), and carbonates (1150 cm^{-1})[52,53] in the interaction of CO with ceria have been reported. In many previous studies involving cerium oxide and aluminum oxide supports, the focus has been on the cerium oxide and the role of aluminum oxide has been under-emphasized.

3.4. Efficiency of PdO/CeO_x-Al_2O_3 catalysts

Catalytic efficiency is a key factor in industrial processes, influencing operational costs, product quality, and environmental impact. The catalytic efficiency depends on activity, activation energy, reaction rate, stability, and selectivity. The turnover frequency (TOF) is a good measure of catalytic efficiency. However, we could not calculate TOF since Pd dispersion measurements were unreliable due to the reduction of PdO by CO. Hence, we estimated the catalytic efficiency from CO activity, long-term stability, and durability data (Fig. 5 and 6). The fresh 3 wt% PdO/6 wt% CeO_x/γ-Al_2O_3 (PdO/CA) catalyst reached 100% CO conversion at 120 °C with a low activation energy (Fig. 5). Preliminary activity experiments with a 1 wt% PdO/6 wt% CeO_x/γ-Al_2O_3 catalyst made by the same method showed T_{50} and T_{100} at 115 °C and 250 °C, respectively, showing the efficiency of the catalyst with a lower Pd loading. The 3 PdO/CA fresh and spent catalysts maintained 100% CO conversion at higher temperatures (200–500 °C) and over long duration (48 h) and displayed high stability and 100% selectivity for CO_2 as the only product. These results show high efficiency and reusability of the as-synthesized $PdO/CeO_x/\gamma$-Al_2O_3 (PdO/CA) catalysts within the limits of laboratory-scale measurements. The evidence from XPS showed the presence of 25–29% adsorbed water in the PdO/CA catalysts and the dual support even after calcining at 500 °C (Fig. 4 and Table S6). The high activity and stability of the catalyst in the presence of adsorbed water suggests a possibility that the catalyst may be water resistant.

Several researchers investigated methane oxidation with similar $PdO/CeO_2/Al_2O_3$ catalysts synthesized by wetness impregnation and related methods.[24,54–56] The catalysts containing 1–4% PdO and 10–20% CeO_2 and balance Al_2O_3 were effective with 90% methane conversion at 260–600 °C. The catalytic activity of $PdO/CeO_2/Al_2O_3$ catalysts for CO and methane oxidation indicates the efficiency of such catalysts as prospective automotive catalysts.

The CO oxidation by ceria/alumina-supported PdO catalysts was complicated by reduction of PdO by CO and the onset of MTL. Several studies on CO oxidation by Pd/alumina and Pd/ceria catalysts contributed to the understanding of the role of active species and reaction mechanism.[8,25,26,35,46,57] Similarly, many researchers contributed to the development of such catalysts for real-life applications.[1,2,16,17,32] Our study is a modest attempt in this direction. The study has limitations and opens possibilities for testing activity at elevated temperatures, water and sulfur dioxide resistance, and MTL under harsh environmental conditions.

4. Conclusions

A $PdO/CeO_x/\gamma\text{-}Al_2O_3$ (PdO/CA) fresh catalyst synthesized by a combination of conventional wetness and vortex methods showed unique properties including high surface area and pore diameter, which are characteristic of mesoporous materials and PdO(101) nanoparticles (1–5 nm) dispersed over the mesoporous $CeO_x/\gamma\text{-}Al_2O_3$ dual support. Both the fresh and spent catalysts showed excellent low-temperature CO oxidation activity with T_{50} of 80–90 °C and T_{90} of 110 °C. Pd (101), CeO_2 (111) and $\gamma\text{-}Al_2O_3$ are identified by X-ray diffraction, high-resolution transmission electron microscopy (HRTEM) and X-ray photoelectron spectroscopy. CO adsorption and *in situ* DRIFTS measurements show CO adsorption on PdO(101), reduction of PdO by CO, and the presence of hydroperoxyl (*O–O–H) intermediate and adsorbed water on the fresh and reduced catalysts as well as on the support. The proposed mechanism involves formation of a hydroperoxyl intermediate by the protonation of adsorbed O_2 and transfer to a CO molecule adsorbed on a PdO site to form a bicarbonate intermediate. The experimental data support a Langmuir–Hinshelwood mechanism for CO oxidation through the hydroperoxyl-bicarbonate pathway. The CO oxidation shows mass transfer limitations (MTLs) due to internal diffusion at 80–200 °C but the CO conversion keeps on increasing in this temperature range. The fresh and spent catalysts seem to have high intrinsic catalytic activity independent of the MTL, as indicated by high conversion at low temperatures and the intrinsic activity may overcome the mass transfer limitations due to internal diffusion. The research study shows the promise of an efficient and stable $PdO/CeO_x/\gamma\text{-}Al_2O_3$ catalyst synthesized by a simple and replicable method for low-temperature CO oxidation under lean and dry conditions. The study also provides scope for further research on oxygen and CO activation, activity and stability, water and sulfur dioxide resistance, and MTLs under harsh environmental conditions and at elevated temperatures of a catalytic converter.

Author contributions

Anil C. Banerjee: writing – original draft, writing – review & editing, methodology, investigation, formal analysis, data curation, conceptualization, project administration. Isaac T. Olowookere: writing – review & editing, methodology, investigation, formal analysis, data curation, visualization. Devon Cushing: methodology, investigation, formal analysis, data curation, visualization. Emily Knox: methodology, investigation, data curation. Teriana Jackson: methodology, investigation, data curation. Scott Bamonte: methodology, investigation, formal analysis, data curation, visualization. Santiago T. Salamanca: methodology, investigation, formal analysis, data curation, visualization. Abiodun Aderibigbe: methodology, investigation, formal analysis, data curation, visualization. Dilshan Silva: methodology, investigation, formal analysis, data curation, visualization. Steven L. Suib: writing – review & editing, resources, project administration, funding acquisition.

Conflicts of interest

There are no conflicts to declare.

Data availability

The data that support the findings of this study are provided in the manuscript and Supplementary Information (SI). Additional data are available from the corresponding author upon reasonable request.

Supplementary information: Fig. S1–S7, Tables S1–S10, MTL calculations. See DOI: https://doi.org/10.1039/d5ra06192j.

Acknowledgements

The support provided by the Institute of Materials Science, the Center for Advanced Microscopy and Materials Analysis (CAMMA) and NEUCORSE at the University of Connecticut and by Columbus State University for internal faculty and student research grants is acknowledged. Thanks to Ojelade Opeyemi at the School of Chemical and Biomedical Engineering, Georgia Institute of Technology for CO-TPD experiments.

References

1 S. Wang, X. Li, C. Lai, Y. Zhang, X. Lin and S. Ding, Recent advances in noble metal-based catalysts for CO oxidation, *RSC Adv.*, 2024, **14**, 30566–30581.
2 C. Huang, W. Shan, Z. Lian, Y. Zhang and H. He, Recent advances in three-way catalysts of natural gas vehicles, *Catal. Sci. Technol.*, 2020, **10**, 6407–6419.
3 S. Royer and D. Duprez, Catalytic Oxidation of Carbon Monoxide over Transition Metal Oxides, *ChemCatChem*, 2011, **3**, 24–65.
4 X. Wang, C. Huang, B. Wu, W. Yang, Y. Zhang, Y. Xu, Y. Jiao, L. Zhong and J. Wang, A Pt Catalyst with Enhanced Three-Way Catalytic Activity Supported on CeO_2 Modified with

Al_2O_3 for Natural Gas Vehicles, *Ind. Eng. Chem. Res.*, 2025, **64**, 5854–5863.

5 K. Murata, E. Eleeda, J. Ohyama, Y. Yamamoto, S. Arai and A. Satsuma, Identification of active sites in CO oxidation over a Pd/Al_2O_3 catalyst, *Phys. Chem. Chem. Phys.*, 2019, **21**, 18128–18137.

6 A. Satsuma, K. Osaki, M. Yanagihara, J. Ohyama and K. Shimizu, Activity controlling factors for low-temperature oxidation of CO over supported Pd catalysts, *Appl. Catal., B*, 2013, **132–133**, 511–518.

7 P. Canton, G. Fagherazzi, M. Battagliarin, F. Menegazzo, F. Pinna and N. Pernicone, Pd/CO average chemisorption stoichiometry in highly dispersed supported Pd/γ-Al2O3 catalysts, *Langmuir*, 2002, **18**, 6530–6535.

8 E. J. Peterson, A. T. DeLaRiva, S. Lin, R. S. Johnson, H. Guo, J. T. Miller, J. Hun Kwak, C. H. F. Peden, B. Kiefer, L. F. Allard, F. H. Ribeiro and A. K. Datye, Low-temperature carbon monoxide oxidation catalysed by regenerable atomically dispersed palladium on alumina, *Nat. Commun.*, 2014, **5**, 4885.

9 K. Zorn, S. Giorgio, E. Halwax, C. R. Henry, H. Grönbeck and G. Rupprechter, CO Oxidation on Technological Pd–Al_2O_3 Catalysts: Oxidation State and Activity, *J. Phys. Chem. C*, 2011, **115**, 1103–1111.

10 A. I. Boronin, E. M. Slavinskaya, I. G. Danilova, R. V. Gulyaev, Y. I. Amosov, P. A. Kuznetsov, I. A. Polukhina, S. V. Koscheev, V. I. Zaikovskii and A. S. Noskov, Investigation of palladium interaction with cerium oxide and its state in catalysts for low-temperature CO oxidation, *Catal. Today*, 2009, **144**, 201–211.

11 K. Ma, W. Liao, W. Shi, F. Xu, Y. Zhou, C. Tang, J. Lu, W. Shen and Z. Zhang, Ceria-supported Pd catalysts with different size regimes ranging from single atoms to nanoparticles for the oxidation of CO, *J. Catal.*, 2022, **407**, 104–114.

12 S. Xie, L. Liu, Y. Lu, C. Wang, S. Cao, W. Diao, J. Deng, W. Tan, L. Ma, S. N. Ehrlich, Y. Li, Y. Zhang, K. Ye, H. Xin, M. Flytzani-Stephanopoulos and F. Liu, Pt Atomic Single-Layer Catalyst Embedded in Defect-Enriched Ceria for Efficient CO Oxidation, *J. Am. Chem. Soc.*, 2022, **144**, 21255–21266.

13 M. Cargnello, V. V. T. Doan-Nguyen, T. R. Gordon, R. E. Diaz, E. A. Stach, R. J. Gorte, P. Fornasiero and C. B. Murray, Control of metal nanocrystal size reveals metal-support interface role for ceria catalysts, *Science*, 2013, **341**, 771–773.

14 S. Xie, Y. Lu, K. Ye, W. Tan, S. Cao, C. Wang, D. Kim, X. Zhang, J. Loukusa, Y. Li, Y. Zhang, L. Ma, S. N. Ehrlich, N. S. Marinkovic, J. Deng, M. Flytzani-Stephanopoulos and F. Liu, Enhancing the Carbon Monoxide Oxidation Performance through Surface Defect Enrichment of Ceria-Based Supports for Platinum Catalyst, *Environ. Sci. Technol.*, 2024, **58**, 12731–12741.

15 D. Gashnikova, F. Maurer, M. R. Bauer, S. Bernart, J. Jelic, M. Lützen, C. B. Maliakkal, P. Dolcet, F. Studt, C. Kübel, C. D. Damsgaard, M. Casapu and J. D. Grunwaldt, Lifecycle of Pd Clusters: Following the Formation and Evolution of Active Pd Clusters on Ceria During CO Oxidation by In Situ/Operando Characterization Techniques, *ACS Catal.*, 2024, 14871–14886.

16 S. Xie, Z. Wang, W. Tan, Y. Zhu, S. Collier, L. Ma, S. N. Ehrlich, P. Xu, Y. Yan, T. Xu, J. Deng and F. Liu, Highly Active and Stable Palladium Catalysts on Novel Ceria-Alumina Supports for Efficient Oxidation of Carbon Monoxide and Hydrocarbons, *Environ. Sci. Technol.*, 2021, **55**, 7624–7633.

17 L. Li, N. Zhang, R. Wu, L. Song, G. Zhang and H. He, Comparative Study of Moisture-Treated Pd@CeO2/Al2O3 and Pd/CeO2/Al2O3 Catalysts for Automobile Exhaust Emission Reactions: Effect of Core-Shell Interface, *ACS Appl. Mater. Interfaces*, 2020, **12**, 10350–10358.

18 M. Cargnello, N. L. Wieder, T. Montini, R. J. Gorte and P. Fornasiero, Synthesis of dispersible Pd@CeO2 core-shell nanostructures by self-assembly, *J. Am. Chem. Soc.*, 2010, **132**, 1402–1409.

19 M. Fernández, F. Fernández-García, A. Martínez-Arias, L. N. Salamanca, J. M. Coronado, J. A. Anderson, J. C. Conesa and J. Soria, Influence of Ceria on Pd Activity for the CO + O_2 Reaction, *J. Catal.*, 1999, **187**, 474–485.

20 R. S. Monteiro, L. C. Dieguez and M. Schmal, The role of Pd precursors in the oxidation of carbon monoxide over ceria, *Catal. Today*, 2001, **65**, 77–89.

21 S. Bensaid, F. A. Deorsola, D. L. Marchisio, N. Russo and D. Fino, Flow field simulation and mixing efficiency assessment of the multi-inlet vortex mixer for molybdenum sulfide nanoparticle precipitation, *Chem. Eng. J.*, 2014, **238**, 66–77.

22 P. Jiang, W. S. Kim and T. Yu, Effective Dispersion of CuPd Alloy Nanoparticles Using the Taylor Vortex Flow for the Preparation of Catalysts with Relatively Clean Surfaces, *ACS Appl. Nano Mater.*, 2022, **5**, 9604–9614.

23 D. R. Fertal, M. Monai, L. Proaño, M. P. Bukhovko, J. Park, Y. Ding, B. M. Weckhuysen and A. C. Banerjee, Calcination temperature effects on Pd/alumina catalysts: Particle size, surface species and activity in methane combustion, *Catal. Today*, 2021, **382**, 120–129.

24 D. R. Fertal, M. P. Bukhovko, Y. Ding, M. Z. Billor and A. C. Banerjee, Particle size and pdo–support interactions in pdo/ceo2-γ Al_2O_3 catalysts and effect on methane combustion, *Catalysts*, 2020, **10**, 1–16.

25 G. Spezzati, Y. Su, J. P. Hofmann, A. D. Benavidez, A. T. DeLaRiva, J. McCabe, A. K. Datye and E. J. M. Hensen, Atomically dispersed Pd-O species on CeO2(111) as highly active sites for low-temperature CO oxidation, *ACS Catal.*, 2017, **7**, 6887–6891.

26 G. Spezzati, A. D. Benavidez, A. T. DeLaRiva, Y. Su, J. P. Hofmann, S. Asahina, E. J. Olivier, J. H. Neethling, J. T. Miller, A. K. Datye and E. J. M. Hensen, CO oxidation by Pd supported on CeO2(100) and CeO2(111) facets, *Appl. Catal., B*, 2019, **243**, 36–46.

27 S. Colussi, A. Trovarelli, G. Groppi and J. Llorca, The effect of CeO2 on the dynamics of Pd-PdO transformation over Pd/Al2O3 combustion catalysts, *Catal. Commun.*, 2007, **8**, 1263–1266.

28 E. A. Lashina, E. M. Slavinskaya, N. A. Chumakova, O. A. Stonkus, R. V. Gulyaev, A. I. Stadnichenko, G. A. Chumakov, A. I. Boronin and G. V. Demidenko, Self-sustained oscillations in CO oxidation reaction on PdO/Al2O3 catalyst, *Chem. Eng. Sci.*, 2012, **83**, 149–158.

29 J. F. Weaver, J. Choi, V. Mehar and C. Wu, Kinetic coupling among metal and oxide phases during CO oxidation on partially reduced PdO(101): Influence of gas-phase composition, *ACS Catal.*, 2017, **7**, 7319–7331.

30 C. M. Goodwin, M. Shipilin, S. Albertin, U. Hejral, P. Lömker, H. Y. Wang, S. Blomberg, D. Degerman, C. Schlueter, A. Nilsson, E. Lundgren and P. Amann, The Structure of the Active Pd State during Catalytic Carbon Monoxide Oxidization, *J. Phys. Chem. Lett.*, 2021, **12**, 4461–4465.

31 M. M. Montemore, M. A. van Spronsen, R. J. Madix and C. M. Friend, O_2 Activation by Metal Surfaces: Implications for Bonding and Reactivity on Heterogeneous Catalysts, *Chem. Rev.*, 2018, **118**, 2816–2862.

32 J. Zhang, M. Shu, Y. Niu, L. Yi, H. Yi, Y. Zhou, S. Zhao, X. Tang and F. Gao, Advances in CO catalytic oxidation on typical noble metal catalysts: Mechanism, performance and optimization, *Chem. Eng. J.*, 2024, **495**, 153523.

33 A. D. Allian, K. Takanabe, K. L. Fujdala, X. Hao, T. J. Truex, J. Cai, C. Buda, M. Neurock and E. Iglesia, Chemisorption of CO and mechanism of CO oxidation on supported platinum nanoclusters, *J. Am. Chem. Soc.*, 2011, **133**, 4498–4517.

34 G. Li, L. Li, Y. Yuan, J. Shi, Y. Yuan, Y. Li, W. Zhao and J. Shi, Highly efficient mesoporous Pd/CeO2 catalyst for low temperature CO oxidation especially under moisture condition, *Appl. Catal., B*, 2014, **158–159**, 341–347.

35 Y. Kim, H. Lee and J. H. Kwak, Mechanism of CO Oxidation on Pd/CeO_2 (100): The Unique Surface-Structure of CeO_2 (100) and the Role of Peroxide, *ChemCatChem*, 2020, **12**, 5164–5172.

36 S. Colussi, A. Trovarelli, E. Vesselli, A. Baraldi, G. Comelli, G. Groppi and J. Llorca, Structure and morphology of Pd/Al2O3 and Pd/CeO 2/Al2O3 combustion catalysts in Pd-PdO transformation hysteresis, *Appl. Catal., A*, 2010, **390**, 1–10.

37 M.-Y. Wey, H.-H. Tseng, Y.-S. Liang, Y.-C. Chang and C.-Y. Lu, Effects of metal precursor in the sol–gel synthesis on the physicochemical properties of Pd/Al2O3–CeO2 catalyst: CO oxidation, *J. Non-Cryst. Solids*, 2006, **352**, 2166–2172.

38 N. L. Wieder, M. Cargnello, K. Bakhmutsky, T. Montini, P. Fornasiero and R. J. Gorte, Study of the water-gas-shift reaction on Pd@CeO2/Al 2O3 core-shell catalysts, *J. Phys. Chem. C*, 2011, **115**, 915–919.

39 R. M. Al Soubaihi, K. M. Saoud, F. Ye, M. T. Zar Myint, S. Saeed and J. Dutta, Synthesis of hierarchically porous silica aerogel supported Palladium catalyst for low-temperature CO oxidation under ignition/extinction conditions, *Microporous Mesoporous Mater.*, 2020, **292**, 109758.

40 S. W. Chee, J. M. Arce-Ramos, W. Li, A. Genest and U. Mirsaidov, Structural changes in noble metal nanoparticles during CO oxidation and their impact on catalyst activity, *Nat. Commun.*, 2020, **11**, 2133.

41 Z. Zhao, D. Xiao, K. Chen, R. Wang, L. Liang, Z. Liu, I. Hung, Z. Gan and G. Hou, Nature of Five-Coordinated Al in γ-Al2O3 Revealed by Ultra-High-Field Solid-State NMR, *ACS Cent. Sci.*, 2022, **8**, 796–803.

42 X. Zhang, W. Li, Z. Zhou, K. Chen, M. Wu and L. Yuan, High dispersed Pd supported on CeO2 (1 0 0) for CO oxidation at low temperature, *Mol. Catal.*, 2021, **508**, 111580.

43 P. J. Schmitz, R. K. Usmen, C. R. Peters, G. W. Graham and R. W. McCabe, Effect of calcination temperature on Al2O3-supported CeO2: complementary results from XRD and XPS, *Appl. Surf. Sci.*, 1993, **72**, 181–187.

44 M. Wilklow-Marnell and W. D. Jones, Catalytic oxidation of carbon monoxide by A-alumina supported 3 nm cerium dioxide nanoparticles, *Mol. Catal.*, 2017, **439**, 9–14.

45 S. Damyanova, C. A. Perez, M. Schmal and J. M. C. Bueno, Characterization of ceria-coated alumina carrier, *Appl. Catal., A*, 2002, **234**, 271–282.

46 B. Liu, J. Liu, T. Li, Z. Zhao, X.-Q. Gong, Y. Chen, A. Duan, G. Jiang and Y. Wei, Interfacial Effects of CeO_2 -Supported Pd Nanorod in Catalytic CO Oxidation: A Theoretical Study, *J. Phys. Chem. C*, 2015, **119**, 12923–12934.

47 A. C. Banerjee, L. Proaño, A. Alvarez, I. Rogers, J. Park, M. Montgomery, M. Z. Billor, B. M. Weckhuysen and M. Monai, Stabilizing Pd-cerium oxide-aluminum oxide catalysts for methane oxidation by reduction pretreatments, *Catal. Sci. Technol.*, 2023, **14**, 153–163.

48 J. T. García-Sánchez, R. Valderrama-Zapata, L. F. Acevedo-Córdoba, D. Pérez-Martínez, S. Rincón-Ortiz and V. G. Baldovino-Medrano, Calculation of Mass Transfer Limitations for a Gas-Phase Reaction in an Isothermal Fixed Bed Reactor: Tutorial and Sensitivity Analysis, *ACS Catal.*, 2023, **13**, 6905–6918.

49 T. M. Tran-Thuy, C. C. Chen and S. D. Lin, Spectroscopic Studies of How Moisture Enhances CO Oxidation over Au/BN at Ambient Temperature, *ACS Catal.*, 2017, **7**, 4304–4312.

50 L. Caulfield, E. Sauter, H. Idriss and C. Wöll, Tracking the Redox Properties of CeO_2 Powders by Infrared Spectroscopy: Monitoring the Defect States by O_2 Adsorption and the Ce^{3+} Spin–Orbit Transition, *J. Phys. Chem. C*, 2025, **129**, 1228–1233.

51 J. Guzman, S. Carrettin and A. Corma, Spectroscopic Evidence for the Supply of Reactive Oxygen during CO Oxidation Catalyzed by Gold Supported on Nanocrystalline CeO_2, *J. Am. Chem. Soc.*, 2005, **127**, 3286–3287.

52 G. N. Vayssilov, M. Mihaylov, P. S. Petkov, K. I. Hadjiivanov and K. M. Neyman, Reassignment of the vibrational spectra of carbonates, formates, and related surface species on ceria: A combined density functional and infrared spectroscopy investigation, *J. Phys. Chem. C*, 2011, **115**, 23435–23454.

53 M. Nolan and G. W. Watson, The surface dependence of CO adsorption on ceria, *J. Phys. Chem. B*, 2006, **110**, 16600–16606.

54 X. Liu, J. Liu, F. Geng, Z. Li, P. Li and W. Gong, Synthesis and properties of PdO/CeO 2-Al 2O 3 catalysts for methane combustion, *Front. Chem. Sci. Eng.*, 2012, **6**, 34–37.
55 T. Tabakova, B. Grahovski, Y. Karakirova, P. Petrova, A. M. Venezia, L. F. Liotta and S. Todorova, Effect of Support on Complete Hydrocarbon Oxidation over Pd-Based Catalysts, *Catalysts*, 2025, **15**, 110.
56 L. M. T. Simplício, S. T. Brandão, D. Domingos, F. Bozon-Verduraz and E. A. Sales, Catalytic combustion of methane at high temperatures: Cerium effect on PdO/Al2O3 catalysts, *Appl. Catal., A*, 2009, **360**, 2–7.
57 B. Wang, Q. Yang, B. Li, H. Ma, Y. Xuan, C. Gao, Y. Liang, K. Zhang, Q. Chang, O. Broesicke, H. Wang, D. Wang, T. Luan, K. Han, C. Lu and J. Crittenden, Heterostructure-strengthened metal-support interaction of single-atom Pd catalysts enabling efficient oxygen activation for CO and VOC oxidation, *Appl. Catal., B*, 2023, **332**, 122753.